Supplementary material, methods, and discussion

CLEANING METHODS AND MG/CA-T CALIBRATION

Cleaning techniques for foraminifera for Mg/Ca analyses include water and methanol rinses, but techniques vary as to whether they include oxidative and reductive steps [*Boyle and Keigwin*, 1985/6; *Rosenthal et al.*, 1997] or only an oxidative step [*Barker et al.*, 2003]. The difference in cleaning technique has been found to affect Mg/Ca ratios. Barker *et al.* [2003] found the reductive step lowers Mg/Ca ratios by approximately 10%, and an interlaboratory comparison study estimated the reductive step lowered Mg/Ca by 15% [*Rosenthal et al.*, 2004]. Recent work by *Arbuszewski et al.* [2010] found the difference to be 8-9%.

Mg/Ca values were converted to temperature using the Anand multispecies equation [*Anand et al.*, 2003] as this calibration is relatively data rich. The equation was adjusted to account for the fact that the Anand calibration was based on foraminifera that had been cleaned only with an oxidative step. We assume the reductive step reduces Mg/Ca values by approximately 10%:

$$\text{Original Anand Multi-species equation: Mg/Ca} = 0.38\exp(0.090T)$$
$$\text{Modified Anand equation: Mg/Ca} + 0.1\text{Mg/Ca} = 0.38e^{0.09T} \text{ or}$$
$$\text{Mg/Ca} = 0.345\exp(0.090T)$$

Mg/Ca samples from cores GeoB10029-4 [*Mohtadi et al.*, 2010], GeoB10038-4 [*Mohtadi et al.*, 2010], MD98-2162 [*Visser et al.*, 2003], MD98-2165 [*Levi et al.*, 2007], MD98-2170 [*Stott et al.*, 2007], MD98-2176 [*Stott et al.*, 2007], MD98-2181 [*Stott et al.*, 2007], and MD01-2390 [*Steinke et al.*, 2008] were converted to

temperature using the Anand multispecies equation. The modified equation was used for samples from GeoB10069-3 and MD78 [*Xu et al.*, 2008]. For cores TR163-22 [*Lea et al.*, 2006], MD97-2141 [*Rosenthal et al.*, 2003], and ME0005A-43JC [*Benway et al.*, 2006] we used the SSTs from the original publication in order to account for the potential effects of dissolution (TR163-22 and MD97-2141) and the use of the through-flow technique (ME0005A-43JC).

$\delta^{18}O_{sw}$ CALCULATIONS

Mg/Ca-based temperature estimates and $\delta^{18}O_{calcite}$ data from the same depth horizons were used to calculate $\delta^{18}O_{sw}$, with the exception of MD01-2390 as Mg/Ca and $\delta^{18}O_{calcite}$ measurements were not made on the same depth horizons in that record. For MD01-2390, data were placed into 200-year bins and then $\delta^{18}O_{sw}$ was calculated.

Following [*Lea et al.*, 2000], the low-light *O. universa* calibration [*Bemis et al.*, 1998] was used to obtain $\delta^{18}O_{sw}$:

Bemis low-light *O. universa* equation: $T(°C) = 16.5 - 4.80(\delta^{18}O_{calcite} - \delta^{18}O_{sw}) - 0.27‰$

For 20-0 kyr before present (BP), the change in $\delta^{18}O_{sw}$ due to continental ice decay was removed using a sea level curve [*Clark and Mix*, 2002] and the corresponding change in the global $\delta^{18}O_{sw}$ of 1.0‰ [*Schrag et al.*, 2002] allowing us to estimate the $\delta^{18}O$ of seawater corrected for ice volume ($\delta^{18}O_{sw-iv}$). For 35-20 kyr BP we used the sea leve curve of *Waelbroeck et al.* [*Waelbroeck et al.*, 2002].

We evaluate the $\delta^{18}O_{sw}$ reconstructions by comparing them to modern water measurements. In each core, we average $\delta^{18}O_{sw}$ samples from 2-0 kyr BP. We plot these "modern" averages against the mean annual World Ocean Atlas 05 salinity [*Antonov et al.*, 2006] from each core location. We compare the resulting $\delta^{18}O_{sw}$/salinity relationship with regional $\delta^{18}O_{sw}$ and salinity data (not the gridded data product) compiled by LeGrande and Schmidt [2006] (Figure 6). For the IndoPacific coretops, the slopes of the reconstructed $\delta^{18}O_{sw}$/salinity (m = 0.48) and the modern water $\delta^{18}O_{sw}$/salinity (m = 0.44) are within error. For the Eastern Equatorial Pacific, the slopes are also very similar (0.22 for the water samples and 0.31 for the foraminifera samples).

In order to calculate our time slice anomalies (Figure 8), all data from 2-0 kyr BP was averaged in each core. This value was used as the "modern" value at each site. For MD97-2141 [*Rosenthal et al.*, 2003] this method was not possible since the most recent 4 kyr of sediment are missing from the core. For this core we used the $\delta^{18}O_{sw}$ value from the closest grid box from the LeGrande and Schmidt [2006] gridded data.

ERROR ANALYSIS ON THE $\delta^{18}O_{sw\text{-}iv}$ ESTIMATES

We estimate the errors of our $\delta^{18}O_{sw\text{-}iv}$ reconstructions by propagating the error introduced by the $\delta^{18}O$-paleotemperature equation, the Mg/Ca-SST calibration, and the removal of global ice volume. For simplicity, we use our instrumental error for all Mg/Ca and $\delta^{18}O_{calcite}$ measurements, even if the data were collected elsewhere.

I. The δ¹⁸O-paleotemperature equation

To solve for $\delta^{18}O_{sw}$, we use the Low Light *O. universa* δ¹⁸O-paleotemperature [*Bemis et al.*, 1998] equation:

T = a + b(δ¹⁸O_calcite − δ¹⁸O_seawater),

rewritten as

δ¹⁸O_sw = -T/b + a/b + δ¹⁸O_calcite

where a = 16.5 ± 0.2°C; b = -4.80 ± 0.16°C. T is determined from Mg/Ca measurements. The errors associated with the conversion to temperature are described in part II.

The errors on the δ¹⁸O-paleotemperature equation were propagated by assuming no covariance among the errors in a, b, T and δ¹⁸O_calcite [*Bevington and Robinson*, 1992]:

$$S_{d^{18}O_{sw}}^2 = \left(\frac{\partial d^{18}O_{sw}}{\partial T}S_T\right)^2 + \left(\frac{\partial d^{18}O_{sw}}{\partial a}S_a\right)^2 + \left(\frac{\partial d^{18}O_{sw}}{\partial b}S_b\right)^2 + \left(\frac{\partial d^{18}O_{sw}}{\partial d^{18}O_{calcite}}S_{d^{18}O_{calcite}}\right)^2$$

where

$$\frac{\P d^{18}O_{sw}}{\P T} = -\frac{1}{b},$$

$$\frac{\P d^{18}O_{sw}}{\P a} = \frac{1}{b},$$

$$\frac{\P d^{18}O_{sw}}{\P b} = \frac{T}{b^2} - \frac{a}{b^2},$$

and

$$\frac{\P d^{18}O_{sw}}{\P d^{18}O_{calcite}} = 1$$

II. Errors on our temperature estimates

We used the values and associated errors on the multispecies equation of Anand *et al.* [2003]:

$$\frac{Mg}{Ca} = be^{aT}$$

b = 0.38 ± 0.02 mmol/mol; a = 0.090 ± 0.003 °C^{-1}

or for the full cleaning equation:

b = 0.345 ± 0.02 mmol/mol; a = 0.090 ± 0.003 °C^{-1}

Our estimate of the instrumental uncertainty of the Mg/Ca measurement was based on running 17 paired samples. These samples were not homogenized prior to

cleaning. The variance ($\sigma^2_{Mg/Ca}$) was 0.21mmol/mol. The above relationship

between Mg/Ca and temperature is solved for T:

$$T = \frac{1}{a}\ln(\frac{Mg}{bCa})$$

This equation is used to propagate the errors in a, b, and Mg/Ca on temperature:

$$S_T^2 = (\frac{\partial T}{\partial a}S_a)^2 + (\frac{\partial T}{\partial b}S_b)^2 + (\frac{\partial T}{\partial Mg/Ca}S_{Mg/Ca})^2$$

where

$$\frac{\partial T}{\partial a} = -\frac{1}{a^2}\ln(\frac{Mg/Ca}{b}),$$

$$\frac{\partial T}{\partial b} = -\frac{1}{ab},$$

and

$$\frac{\partial T}{\partial Mg/Ca} = \frac{1}{a}\frac{1}{Mg/Ca}$$

III. Errors on the global ice volume estimates.

We use estimates of the difference between the Last Glacial Maximum and modern

values of the $\delta^{18}O_{sw}$ ($\Delta\delta^{18}O = 1 \pm 0.1‰$) [*Schrag et al.*, 2002] and sea level ($\Delta SL =$

130 ± 7.5m) [*Clark and Mix*, 2002] to create a scaling factor. We use this scaling

factor, in conjunction with coral reconstruction of deglacial sea level, to estimate

$\delta^{18}O_{sw}$ changes over the course of the deglaciation. We assume the isotopic composition of the melting ice was constant. A comparison of sea level reconstructions shows variance among records [*Hanebuth et al.*, 2000]. We suggest a standard deviation (σ_{SL}) of ± 10m for sea level (SL) is reasonable.

We use the following equation to determine $\delta^{18}O_{ice}$:

$$d^{18}O_{ice}(t) = SL(t)\frac{Dd^{18}O}{DSL}$$

where t is time, SL(t) is the sea level [*Clark and Mix*, 2002], and

$\Delta\delta^{18}O / \Delta SL = 1/130$ ‰/m.

The associated error is estimated from

$$S^2_{d^{18}O_{ice}} = \left(\frac{\partial d^{18}O_{ice}}{\partial SL}S_{SL}\right)^2 + \left(\frac{\partial d^{18}O_{ice}}{\partial Dd^{18}O}S_{Dd^{18}O}\right)^2 + \left(\frac{\partial d^{18}O_{ice}}{\partial DSL}S_{DSL}\right)^2$$

where

$$\frac{\partial d^{18}O_{ice}}{\partial SL} = \frac{Dd^{18}O}{DSL},$$

$$\frac{\partial d^{18}O_{ice}}{\partial Dd^{18}O} = \frac{SL}{DSL},$$

and

$$\frac{\partial d^{18}O_{ice}}{\partial \mathrm{D}SL} = -SL\frac{\mathrm{D}d^{18}O}{(\mathrm{D}SL)^2}$$

IV. Errors on the bin averages

For every record, if there was a single data point in the 500-year bin, the error was simply $\sigma_{\delta 18Osw}$, as described above. In instances were there were multiple $\delta^{18}O_{sw}$ values in a 500-year bin, we calculated the standard deviation in the following manner [*Bevington and Robinson*, 1992], where n is the number of data points in each bin,

$$S^2_{bind^{18}O_{sw}} = \frac{1}{n^2}\sum_{i=1}^{n} S^2_{d^{18}O_{sw}i}$$

The variance on the 500-year bins in the regional stack was determined by summing the square of the variances ($\sigma^2_{bin\delta 18Osw}$) from each binned record.

$$S^2_{averaged^{18}O_{sw}} = \frac{1}{n^2}\sum_{i=1}^{n} S^2_{bind^{18}O_{sw}i}$$

AGE MODELS

All age models are based on previously published planktic foraminifera radiocarbon dates with the exception GeoB10069-3, where we collected new radiocarbon dates (supplementary data). All radiocarbon dates were converted to calendar ages using the Calib 6.0 program, the Marine 09 calibration, and the global

8

reservoir age [*Reimer et al.*, 2009]. The calendar age with the median probability was selected. All dates are listed in supplementary data. Age models for GeoB10069-3, MD98-2162 [*Visser et al.*, 2003], MD98-2165 [*Levi et al.*, 2007], V21-30 [*Koutavas et al.*, 2002], ME0005A-43JC [*Benway et al.*, 2006], TR163-22 [*Lea et al.*, 2006], GeoB10029-4 [*Mohtadi et al.*, 2010], GeoB10038-4 [*Mohtadi et al.*, 2010], MD98-2176 [*Stott et al.*, 2007], MD98-2170 [*Stott et al.*, 2007], and MD01-2390 [*Steinke et al.*, 2008] were created by linearly interpolating between derived calendar ages.

The age models for MD97-2141, MD78, and MD98-2181 were constructed by utilizing the equations listed below.

Polynomial for MD97-2141[*Rosenthal et al.*, 2003]

$y = -0.00000000124x^5 + 0.000001404x^4 - 0.0007356x^3 + 0.1782x^2 + 31.90x + 4314$

$R^2 = 0.979$

Linear fit for MD01-2378 [*Sarnthein et al.*, 2011; *Xu et al.*, 2008] (the intercept was set at 1050, to produce a realistic coretop age)

$y = 48.884x + 1050$

$R^2 = 0.991$

Polynomial for MD98-2181 [*Stott et al.*, 2007]

$y = -0.000000002262x^4 + 0.000004298x^3 + 0.006586x^2 + 4.412x + 107$

$R^2 = 0.997$

PRINCIPAL COMPONENT ANALYSIS AND THE REGIONAL AVERAGE

We computed the arithmetic average of our data using 500-year non-overlapping bins. Data from each record were placed into 500-year bins and averaged. For each time interval we then averaged the averages. We only averaged the cores with data; cores without data were simply excluded from the time bin.

Principal component analysis [*Jolliffe*, 2002] was also used to explore the common features of the $\delta^{18}O_{sw-iv}$. All $\delta^{18}O_{sw-iv}$ reconstructions were placed into 500-year non-overlapping bins. Missing values were replaced with the average value of the record following Marchal *et al.* [2002]. We computed the principal components for the time interval from 1.25 kyr BP to 19.75 kyr BP (Figure 4).

Principal component analysis can be used to determine shared variance among a set a variables [*Rencher*, 1995]. Possibly correlated variables, in this case time series, are converted into new variables, the principal components, that are linearly uncorrelated. The first principal component is a variable that describes the largest portion of shared variance in the time series. The loadings describe how much each time series contributes to a given principal component. By multiplying each time series by its respective loading and summing these modified set of time series, one obtains the corresponding principal component. Several other terms are occasionally used instead of "loadings:" coefficients, pattern coefficients, and empirical orthogonal weights [*Wilks*, 1995].

The second and third principal components (supplementary figure 4)

respectively explain 8% and 9% of the variability. The loadings for the second and

third principal component are shown in supplementary figure 5.

MODEL DESIGN AND HEAT TRANSPORT CALCULATIONS

Model Design: The TraCE-21000 is carried out in a synchronously coupled ocean–

atmosphere–sea ice–land surface climate model without flux adjustment - the

National Center for Atmospheric Research (NCAR) Community Climate System

Model version 3 [*Collins et al.*, 2006], in the version of T31_gx3v5 resolution [*Yeager*

et al., 2006]. The atmospheric model is the CAM3 with horizontal resolution of about

3.75 ° × 3.75 ° and 26 vertical hybrid coordinate levels. The land model is CLM3 with

same resolution as the atmosphere. The ocean model is the NCAR implementation of

POP with vertical z-coordinate and 25 levels. The longitudinal resolution is 3.6

degree and the latitudinal resolution is variable, with finer resolution in the equator

(~0.9 degrees). The sea ice model is the CSIM with same resolution as the ocean

model.

The TraCE-21000 was initialized from an earlier LGM equilibrium simulation

of CCSM3 [*Otto-Bliesner et al.*, 2006] with dynamic vegetation added to reduce the

model drift in the deep ocean. This transient simulation cover the period of 22 ~ 0

ka with realistic changes in boundary conditions and various forcings – the

continental ice sheet and coastlines [*Peltier*, 2004], the orbital forcing (only its long-

term variation [*Berger*, 1978]), the green house gas forcing, including CO_2, CH_4 and

N_2O [*Joos and Spahni*, 2008]) forcing, and the meltwater forcing [*Liu et al.*, 2009],

which was derived from the reconstructed sea level changes in Peltier [2004]. The TraCE-21000 captures many major features of the deglacial climate evolution, for example, cooling during Heinrich event 1(H1), abrupt BA warming and cooling in Younger Dryas (YD) [*Liu et al.*, 2009].

Atmospheric heat transport: Meridional heat transport of the atmosphere at the equator is a zonal sum of the net vertical heat flux between the top and bottom of air column (NVHFLX) at each grid of model. The vertical heat fluxes at top of atmosphere include net solar flux (FSNTOA) and net longwave flux (FLNT). At the bottom of the atmosphere fluxes include sensible heat flux (SHFLX), latent heat flux (LHFLX), net solar flux (FSNS), and net longwave flux (FLNS). The net vertical heat flux of air column at each grid is calculated with the formula:

NVHFLX = FSNTOA – FLNT + SHFLX + LHFLX + FLNS – FSNS

The magnitudes of meridional atmospheric heat transport at all latitudes in this model are similar to the observed ones [*Trenberth and Caron*, 2001].

Oceanic heat transport: Meridional heat transport of the ocean at the equator is a sum of the net meridional heat transport at each grid of the corresponding zonal/vertical section in the model ocean. The net meridional heat transport at ocean each grid is calculated with the meridional velocity (V) and temperature (T), and its magnitude is the difference of VT over one meridional step length with the interpolation of V at V grid to T grid.

The magnitudes of meridional oceanic heat transport at all latitudes in this model are similar to the observed ones [*Trenberth and Caron*, 2001].

## HOLOCENE INTERHEMISPHERIC TEMPERATUR GRADIENT

To calculate the Holocene interhemispheric temperature gradient we used the temperature data found in Fig. S10 of Marcott et al. [2013]. 6 bins were plotted in that figure: 90°N-60°N, 60°N-30°N, 30°N-0°, 90°S-60°S, 60°S-30°S, and 30°S-0°. To create an average temperature for the entire hemisphere, the values in each bin were scaled by the relative surface area encompassed by the bin's latitudinal range: 13.4% for 90°-60°, 36.6% for 60°-30°, and 50% for 30°-0°. The resulting values were then summed to obtain the average temperature for the entire hemisphere.
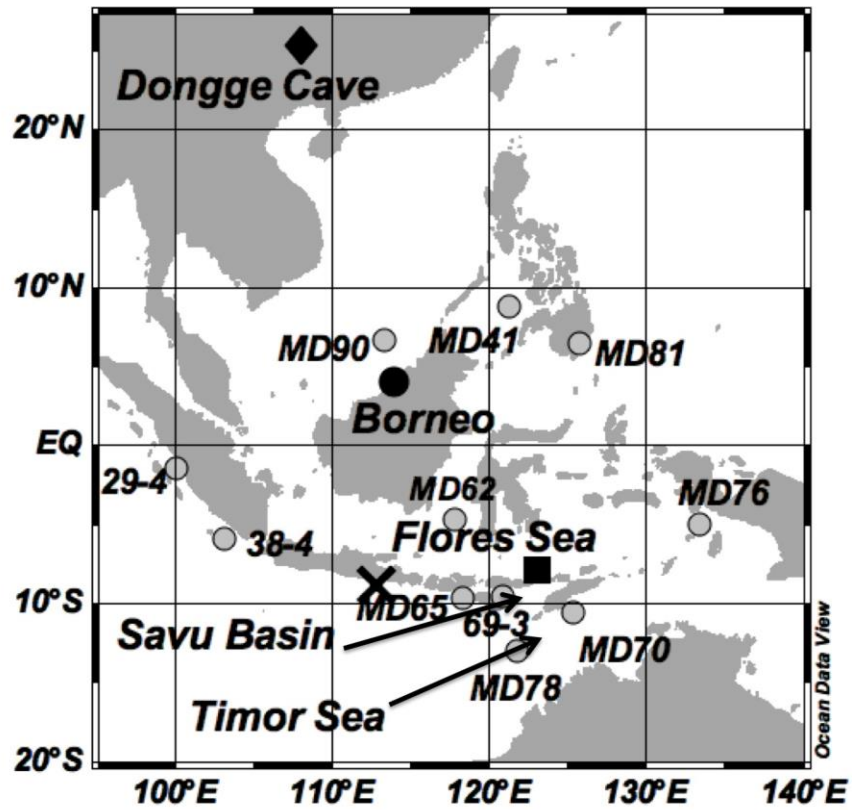
Supplementary Fig. 1. Map of IndoPacific. The locations of the Borneo Cave[*Partin et al.*, 2007] (black filled circle), the Dongge Cave [*Yuan et al.*, 2004] (diamond), VM33-80 [*Muller et al.*, 2012] (square), and GeoB 10053-7 [*Mohtadi et al.*, 2011] (X) are shown. Gray filled circles are the locations of the IndoPacific cores discussed in the main text.
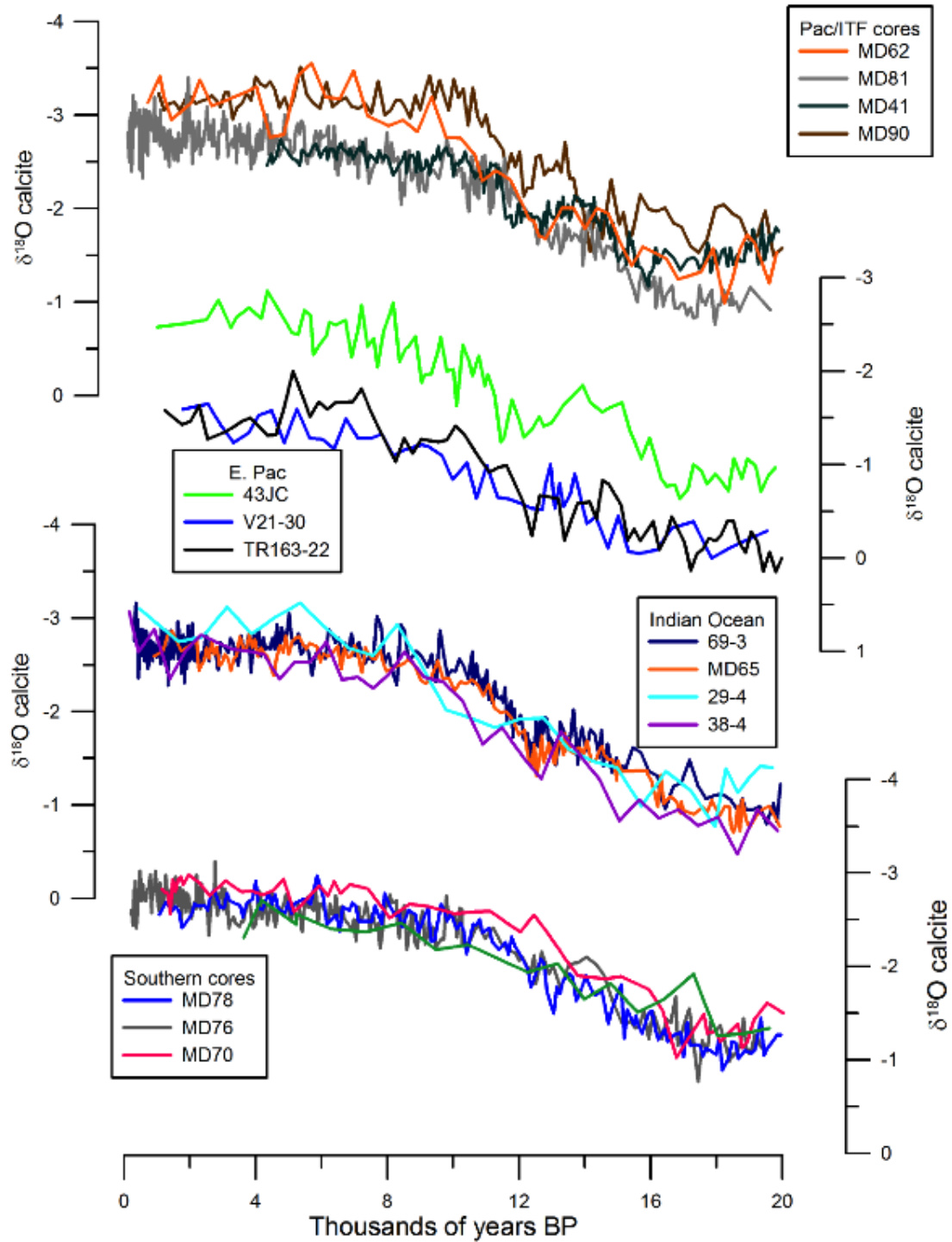
Supplementary Fig. 2. $\delta^{18}O_{calcite}$ data from all cores used in this study. The cores are grouped by region. Note the "southern cores" are not strictly the most southern by latitude, but they are generally to the south (see Table 1) and group together hydrologically as described in the text.
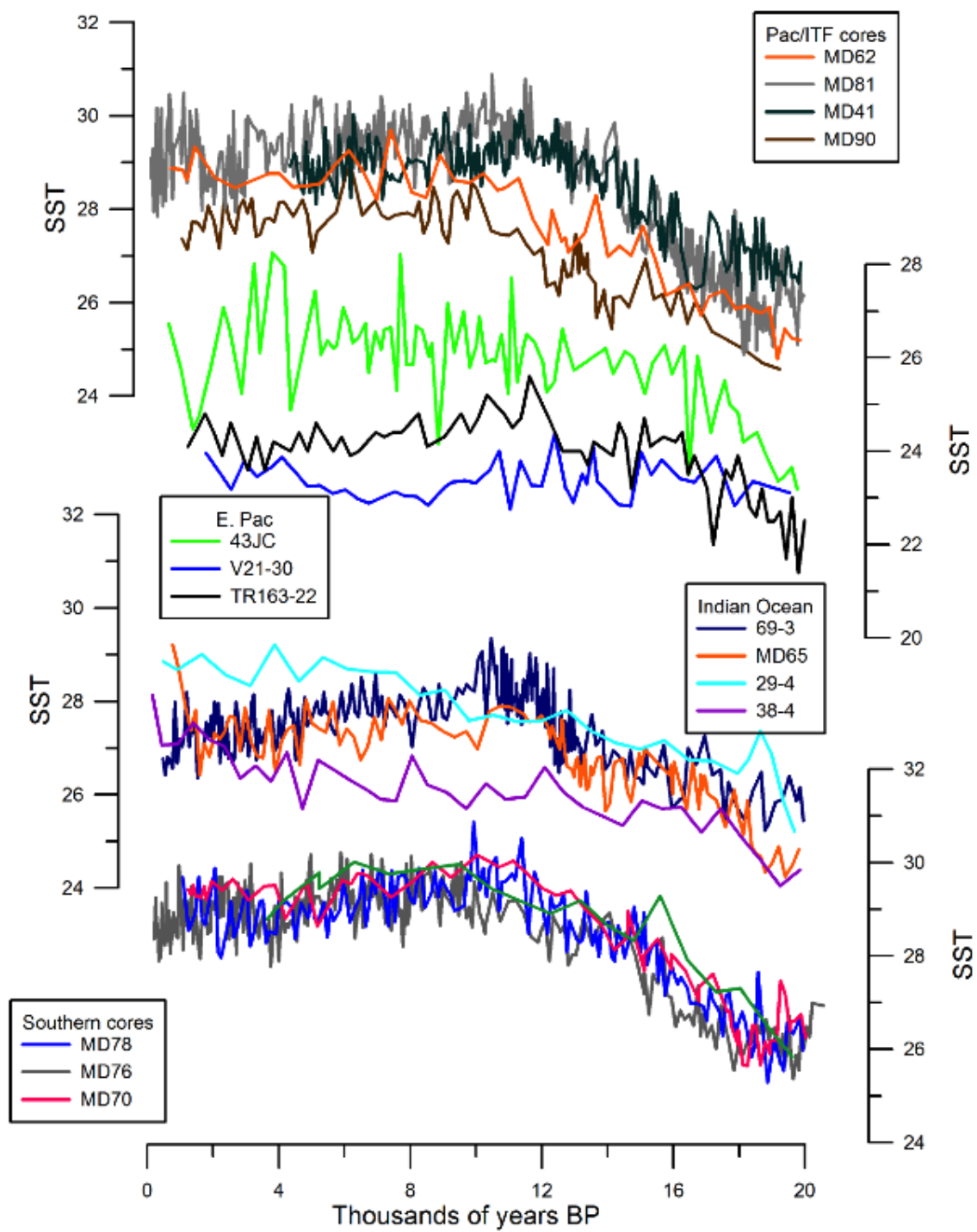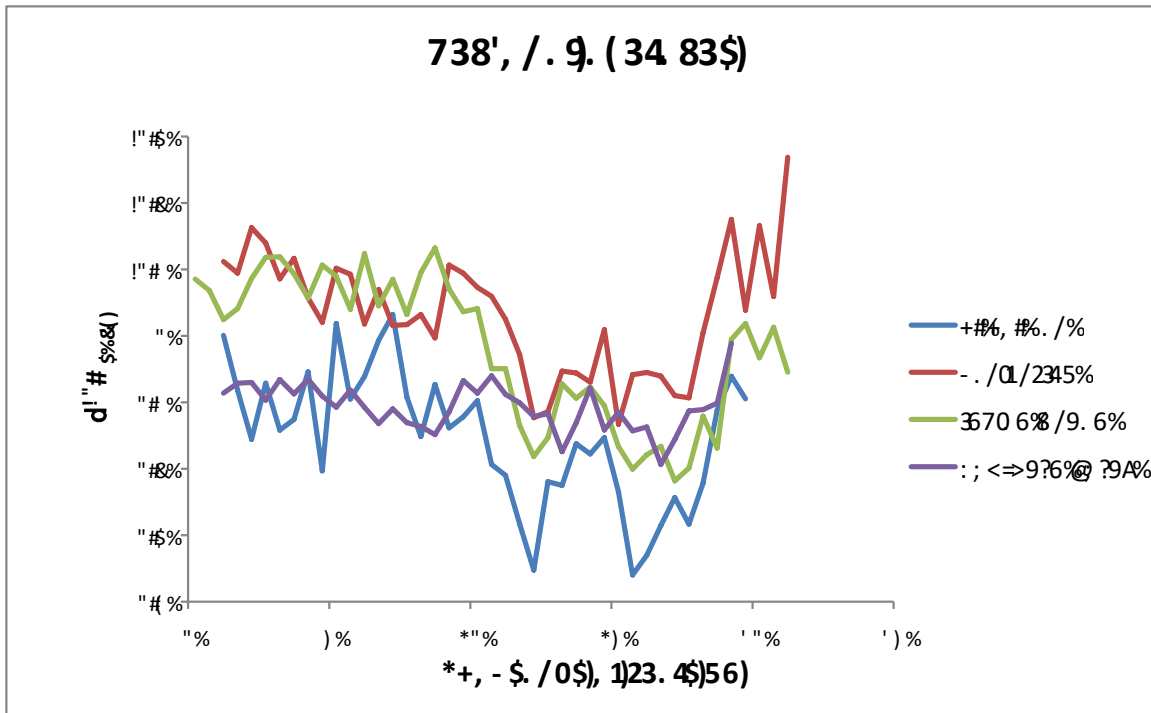
Supplementary Fig. 3. Mg/Ca-based temperature data from all cores used in this study.
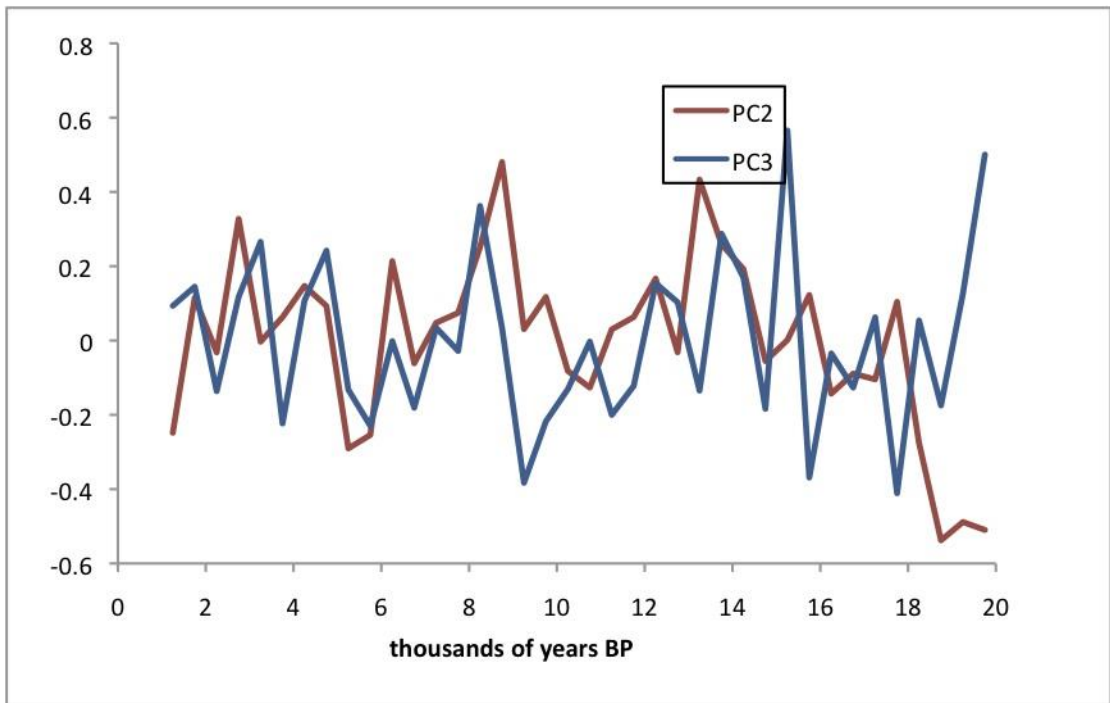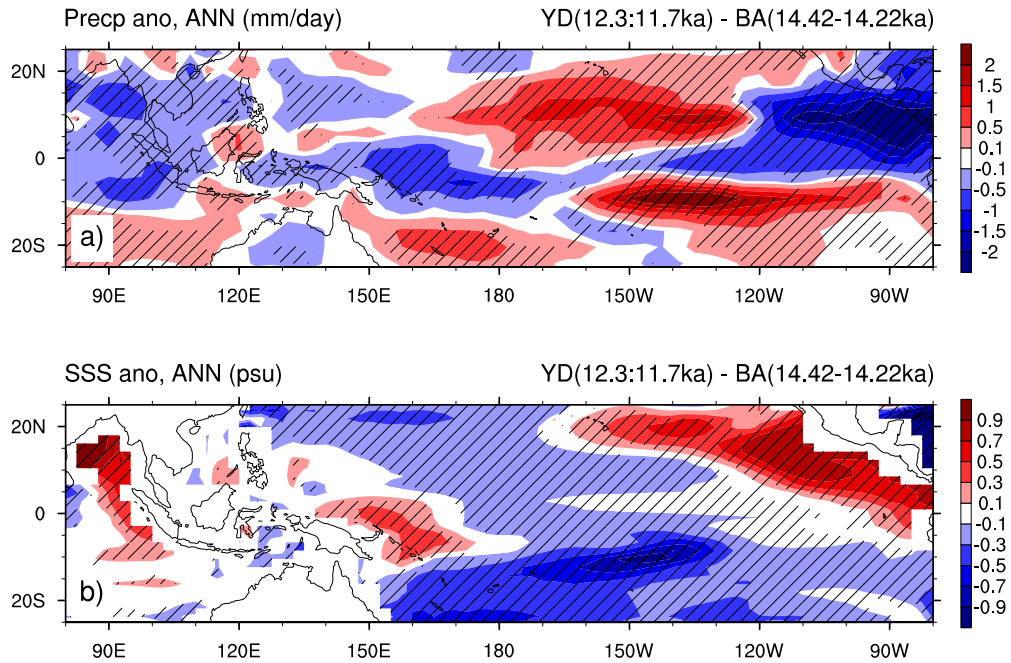
Supplementary Fig. 4. Time series of second and third principal components, which respectively explain 9% and 8% of the variability in the data.
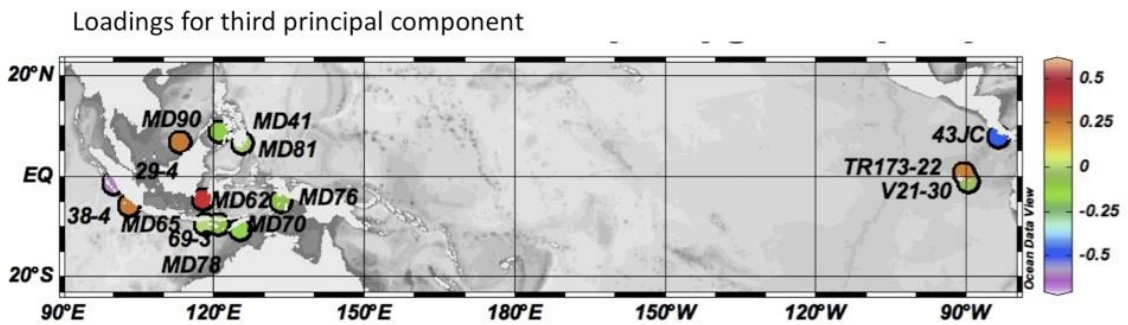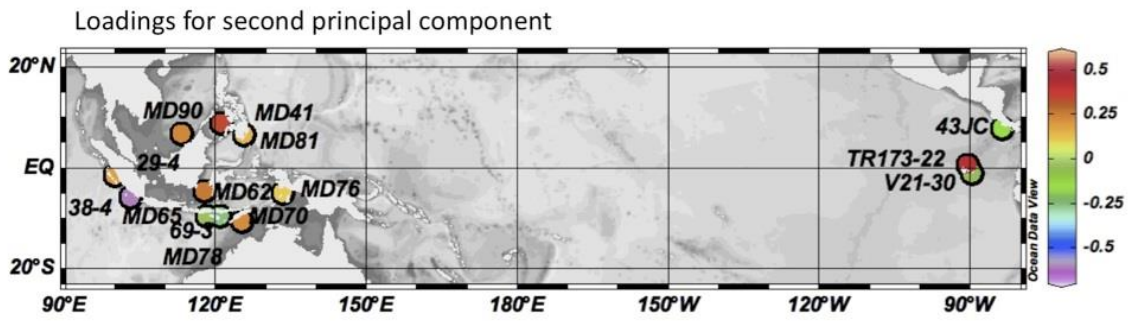
Supplementary Fig. 5. Loadings for the second and third principal component.

Supplementary figure 6: Regional averages of data from figure 2. Data from each core were placed into 500-year bins and then averaged.

Precp ano, ANN (mm/day)   YD(12.3:11.7ka) - BA(14.42-14.22ka)

a)

SSS ano, ANN (psu)   YD(12.3:11.7ka) - BA(14.42-14.22ka)

b)

Supplementary Fig. 7. Results from a transient run of the National Center for Atmospheric Research's Community Climate System Model version 3. Precipitation differences (top) and sea surface salinity difference (bottom) between the simulated Younger Dryas and the Bølling-Allerød are shown. Hashed zones are significant at the 99.9% level.
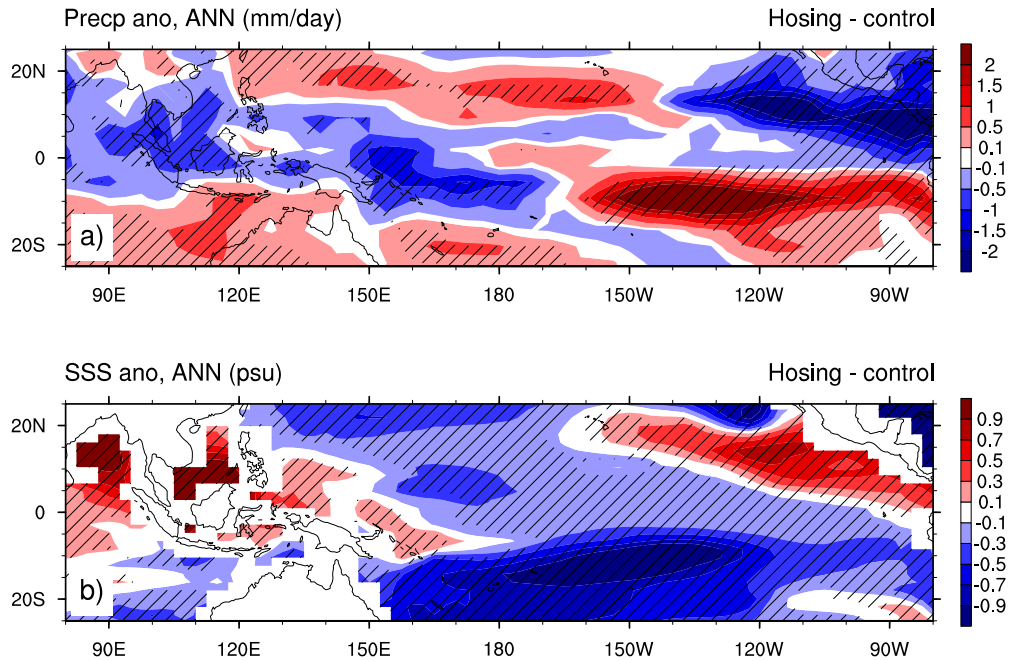
Supplementary Fig. 8. Results from a hosing experiment run on the National Center for Atmospheric Research's Community Climate System Model version 3 [*Otto-Bliesner and Brady*, 2010]. Precipitation differences (top) and sea surface salinity difference (bottom) between the hosing experiment and the preindustrial. Hashed zones are significant at the 99.9% level.
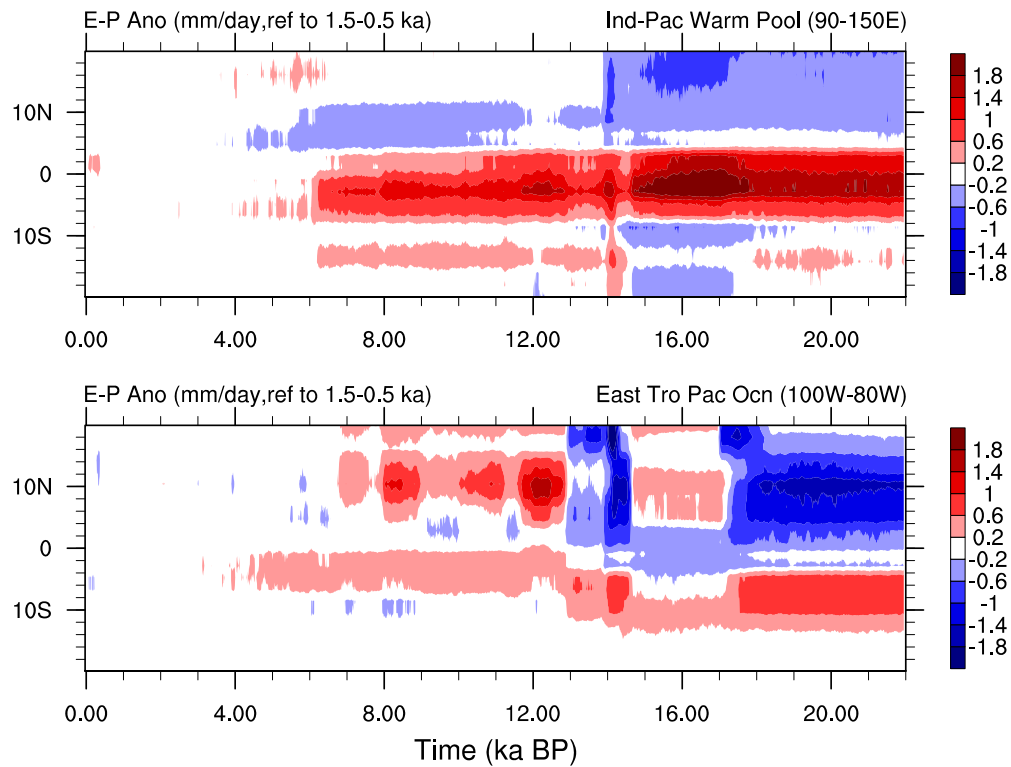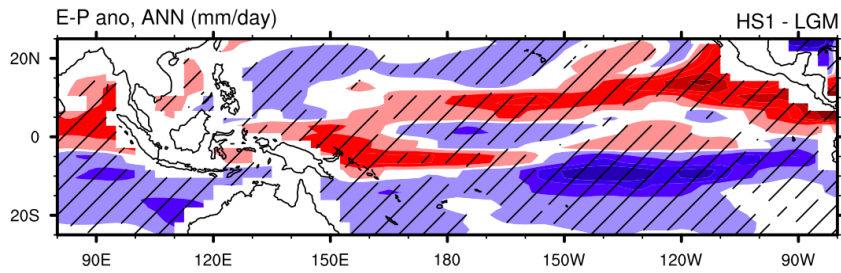
Supplementary Fig. 9. Results from a transient run of the National Center for Atmospheric Research's Community Climate System Model version 3. Zonal mean evaporation-precipitation anomaly for the entire transient simulation (22-0 kyr BP) for 90E-150E (top) and 100W-80W (bottom).
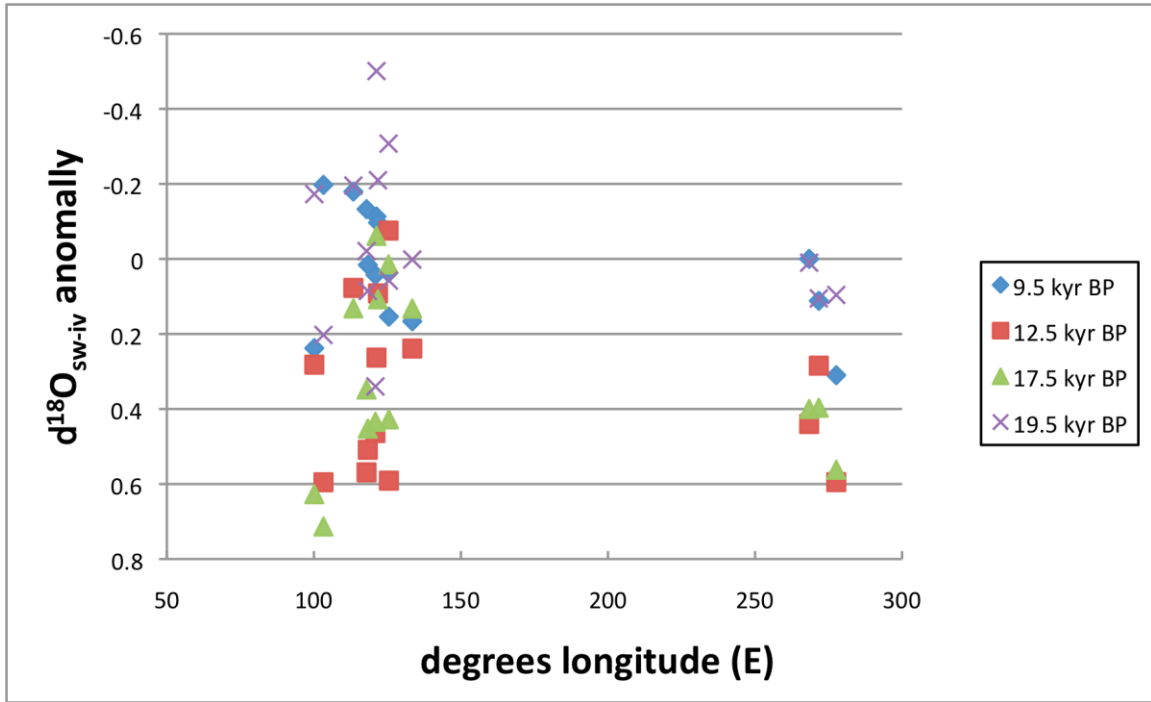
Supplementary Fig. 10. Results from a transient run of the National Center for Atmospheric Research's Community Climate System Model version 3. Annual evaporation minus precipitation differences between the simulated HS1 and the LGM. Hashed zones are significant at the 99.9% level.

Supplementary Fig. 11. 1,000 year averages of $\delta^{18}O_{sw-iv}$ anomalies plotted against longitude for the Early Holocene (9.5 kyr BP), Younger Dryas (12.5 kyr BP), HS1 (17.5 kyr BP), and LGM (19.5 kyr BP).

References:

Anand, P., H. Elderfield, and M. H. Conte (2003), Calibration of Mg/Ca thermometry in planktonic foraminifera from a sediment trap time series, *Paleoceanography*, *18*(2), Pa1050.

Antonov, J. I., R. A. Locarnini, T. P. Boyer, and H. E. Garcia (2006), World Ocean Atlas 2005, Volume 2: Salinity, *NOAA Atlas NESDIS 62*.

Arbuszewski, J., P. B. de Menocal, A. Kaplan, and E. C. Farmer (2010), On the fidelity of shell-derived δ18Oseawater estimates, *Earth and Planetary Science Letters*, *300*(3-4), 185-196,doi: 10.1016/j.epsl.2010.10.035.

Barker, S., M. Greaves, and H. Elderfield (2003), A study of cleaning procedures used for foraminiferal Mg/Ca paleothermometry, *Geochemistry Geophysics Geosystems*, *4*(9), Q8407,doi: 10.1029/2003GC000559.

Bemis, B. E., H. J. Spero, J. Bijma, and D. W. Lea (1998), Reevaluation of the oxygen isotopic composition of planktonic foraminifera: Experimental results and revised paleotemperature equations, *Paleoceanography*, *13*(2), 150-160.

Benway, H. M., A. C. Mix, B. A. Haley, and G. P. Klinkhammer (2006), Eastern Pacific Warm Pool paleosalinity and climate variability: 0-30 kyr, *Paleoceanography*, *21*(3), Pa3008,doi: 10.1029/2005pa001208.

Berger, A. L. (1978), Long-term variations of daily insolation and Quaternary climatic changes, *Journal of the Atmospheric Sciences*, *35*(12), 2362-2367.

Bevington, P. R., and Robinson (1992), Data Reduction and Error Analysis for the Physical Sciences.

Boyle, E. A., and L. D. Keigwin (1985/6), Comparison of Atlantic and Pacific Paleochemical Records for the Last 215,000 Years - Changes in Deep Ocean Circulation and Chemical Inventories, *Earth and Planetary Science Letters*, *76*(1-2), 135-150.

Clark, P. U., and A. C. Mix (2002), Ice sheets and sea level of the Last Glacial Maximum, *Quaternary Science Reviews*, *21*(1-3), 1-7,doi: 10.1016/S0277-3791(01)00118-4.

Collins, W. D., C. M. Bitz, M. L. Blackmon, G. B. Bonan, C. S. Bretherton, J. A. Carton, P. Chang, S. C. Doney, J. J. Hack, and T. B. Henderson (2006), The community climate system model version 3 (CCSM3), *Journal of Climate*, *19*(11), 2122-2143.

Hanebuth, T., K. Stattegger, and P. M. Grootes (2000), Rapid Flooding of the Sunda Shelf: A Late-Glacial Sea-Level Record, *Science*, *288*, 1033-1035,doi: 10.1126/science.288.5468.1033.

Jolliffe, I. T. (2002), *Principal Component Analysis, 2nd edition*, Springer.

Joos, F., and R. Spahni (2008), Rates of change in natural and anthropogenic radiative forcing over the past 20,000 years, *Proceedings of the National Academy of Sciences*, *105*(5), 1425-1430.

Koutavas, A., J. Lynch-Stieglitz, T. M. Marchitto, and J. P. Sachs (2002), El Nino-like pattern in ice age tropical Pacific sea surface temperature, *Science*, *297*(5579), 226-230.

Lea, D. W., D. K. Pak, and H. J. Spero (2000), Climate impact of late quaternary equatorial Pacific sea surface temperature variations, *Science*, *289*(5485), 1719-1724.

Lea, D. W., D. K. Pak, C. L. Belanger, H. J. Spero, M. A. Hall, and N. J. Shackleton (2006), Paleoclimate history of Galapagos surface waters over the last 135,000 yr, *Quaternary Science Reviews*, *25*(11-12), 1152-1167,doi: 10.1016/j.quascirev.2005.11.010.

LeGrande, A. N., and G. A. Schmidt (2006), Global gridded data set of the oxygen isotopic composition in seawater, *Geophysical Research Letters*, *33*(12), L12604,doi: 10.1029/2006GL026011.

Levi, C., L. Labeyrie, F. Bassinot, F. Guichard, E. Cortijo, C. Waelbroeck, N. Caillon, J. Duprat, T. de Garidel-Thoron, and H. Elderfield (2007), Low-latitude hydrological cycle and rapid climate changes during the last deglaciation, *Geochemistry Geophysics Geosystems*, *8*(5), Q05N12,doi: 10.1029/2006GC001514.

Liu, Z., B. L. Otto-Bliesner, F. He, E. C. Brady, R. Tomas, P. U. Clark, A. E. Carlson, J. Lynch-Stieglitz, W. Curry, E. Brook, D. Erickson, R. Jacob, J. Kutzbach, and J. Cheng (2009), Transient Simulation of Last Deglaciation with a New Mechanism for Bølling-Allerød Warming, *Science*, *325*(5938), 310-314,doi: 10.1126/science.1171041.

Marchal, O., I. Cacho, T. F. Stocker, J. O. Grimalt, E. Calvo, B. Martrat, N. Shackleton, M. Vautravers, E. Cortijo, S. van Kreveld, C. Andersson, N. Koc, M. Chapman, L. Sbaffi, J. C. Duplessy, M. Sarnthein, J. L. Turon, J. Duprat, and E. Jansen (2002), Apparent long-term cooling of the sea surface in the northeast Atlantic and Mediterranean during the Holocene, *Quaternary Science Reviews*, *21*(4-6), 455-483.

Marcott, S. A., J. D. Shakun, P. U. Clark, and A. C. Mix (2013), A reconstruction of regional and global temperature for the past 11,300 years, *Science*, *339*(6124), 1198-1201.

Mohtadi, M., S. Steinke, A. Lückge, J. Groeneveld, and E. C. Hathorne (2010), Glacial to Holocene surface hydrography of the tropical eastern Indian Ocean, *Earth and Planetary Science Letters*, *292*, 89-97,doi: 10.1016/j.epsl.2010.01.024.

Mohtadi, M., D. W. Oppo, S. Steinke, J. B. W. Stuut, R. De Pol-Holz, D. Hebbeln, and A. Luckge (2011), Glacial to Holocene swings of the Australian-Indonesian monsoon, *Nature Geoscience*, *4*(8), 540-544,doi: 10.1038/Ngeo1209.

Muller, J., J. McManus, D. W. Oppo, and R. Francois (2012), Strengthening of the Northeast Monsoon over the Flores Sea, Indonesia, at the time of Heinrich event 1, *Geology*, *40*(7), 635-638.

Otto-Bliesner, B. L., E. C. Brady, G. Clauzet, R. Tomas, S. Levis, and Z. Kothavala (2006), Last glacial maximum and Holocene climate in CCSM3, *Journal of Climate*, *19*(11), 2526-2544.

Otto-Bliesner, B. L., and E. C. Brady (2010), The sensitivity of the climate response to the magnitude and location of freshwater forcing: last glacial maximum experiments, *Quaternary Science Reviews*, *29*(1), 56-73.

Partin, J. W., K. M. Cobb, J. F. Adkins, B. Clark, and D. P. Fernandez (2007), Millennial-scale trends in west Pacific warm pool hydrology since the Last Glacial Maximum, *Nature*, *449*(7161), 452-455,doi: 10.1038/Nature06164.

Peltier, W. (2004), Global glacial isostasy and the surface of the ice-age Earth: The ICE-5G (VM2) model and GRACE, *Annu. Rev. Earth Planet. Sci.*, *32*, 111-149.

Reimer, P. J., M. G. L. Baillie, E. Bard, A. Bayliss, J. W. Beck, P. G. Blackwell, C. Bronk Ramsey, C. E. Buck, G. S. Burr, R. L. Edwards, M. Friedrich, P. M. Grootes, T. W.

Guilderson, I. Hajdas, T. J. Heaton, A. G. Hogg, K. A. Hughen, K. F. Kaiser, B. Kromer, F. G. McCormac, S. W. Manning, R. W. Reimer, D. A. Richards, J. R. Southon, S. Talamo, C. S. M. Turney, J. van der Plicht, and C. E. Weyhenmeyer (2009), INTCAL09 AND MARINE09 Radiocarbon age calibration curves, 0–50,000 years cal BP, *Radiocabon*, *51*(4), 1111-1150.

Rencher (1995), *Methods of Multivariate Analysis*, John Wiley & Sons, Inc., New York.

Rosenthal, Y., E. A. Boyle, and N. Slowey (1997), Temperature control on the incorporation of magnesium, strontium, fluorine, and cadmium into benthic foraminiferal shells from Little Bahama Bank: Prospects for thermocline paleoceanography, *Geochimica Et Cosmochimica Acta*, *61*(17), 3633-3643.

Rosenthal, Y., D. W. Oppo, and B. K. Linsley (2003), The amplitude and phasing of climate change during the last deglaciation in the Sulu Sea, western equatorial Pacific, *Geophysical Research Letters*, *30*(8), L1428,doi: 10.1029/2002gl016612.

Rosenthal, Y., S. Perron‚ÄêCashman, C. H. Lear, E. Bard, S. Barker, K. Billups, M. Bryan, M. L. Delaney, P. B. deMenocal, and G. S. Dwyer (2004), Interlaboratory comparison study of Mg/Ca and Sr/Ca measurements in planktonic foraminifera for paleoceanographic research, *Geochemistry, Geophysics, Geosystems*, *5*(4).

Sarnthein, M., P. M. Grootes, A. Holbourn, W. Kuhnt, and H. Kühn (2011), Tropical warming in the timor sea led deglacial antarctic warming and atmospheric CO2 rise by more than 500 yr, *Earth and Planetary Science Letters*, *302*(3-4), 337-348.

Schrag, D. P., J. F. Adkins, K. McIntyre, J. L. Alexander, D. A. Hodell, C. D. Charles, and J. F. McManus (2002), The oxygen isotopic composition of seawater during the Last Glacial Maximum, *Quaternary Science Reviews*, *21*(1-3), 331-342.

Steinke, S., M. Kienast, J. Groeneveld, L. C. Lin, M. T. Chen, and R. Rendle-Buhring (2008), Proxy dependence of the temporal pattern of deglacial warming in the tropical South China Sea: toward resolving seasonality, *Quaternary Science Reviews*, *27*(7-8), 688-700,doi: 10.1016/J.Quascirev.2007.12.003.

Stott, L., A. Timmermann, and R. Thunell (2007), Southern Hemisphere and Deep-Sea Warming Led Deglacial Atmospheric CO2 Rise and Tropical Warming, *Science*, *318*, 435-438,doi: 10.1126/science.1143791.

Trenberth, K. E., and J. M. Caron (2001), Estimates of Meridional Atmosphere and Ocean Heat Transports, *Journal of Climate*, *14*, 3433-3443.

Visser, K., R. Thunell, and L. Stott (2003), Magnitude and timing of temperature change in the Indo-Pacific warm pool during deglaciation, *Nature*, *421*, 152-155.

Waelbroeck, C., L. Labeyrie, E. Michel, J. C. Duplessy, J. F. McManus, K. Lambeck, E. Balbon, and M. Labracherie (2002), Sea-level and deep water temperature changes derived from benthic foraminifera isotopic records, *Quaternary Science Reviews*, *21*(1-3), 295-305.

Wilks, D. S. (1995), *Statistical Methods in the Atmospheric Sciences An Introduction*, 467 pp., Academic Press, San Diego.

Xu, J., A. Holbourn, W. G. Kuhnt, Z. M. Jian, and H. Kawamura (2008), Changes in the thermocline structure of the Indonesian outflow during Terminations I and II, *Earth and Planetary Science Letters*, *273*(1-2), 152-162.

Yeager, S. G., C. A. Shields, W. G. Large, and J. J. Hack (2006), The low-resolution CCSM3, *Journal of Climate*, *19*(11), 2545-2566.

Yuan, D. X., H. Cheng, R. L. Edwards, C. A. Dykoski, M. J. Kelly, M. L. Zhang, J. M. Qing, Y. S. Lin, Y. J. Wang, J. Y. Wu, J. A. Dorale, Z. S. An, and Y. J. Cai (2004), Timing, duration, and transitions of the Last Interglacial Asian Monsoon, *Science*, *304*(5670), 575-578.